ELSEVIER

Contents lists available at ScienceDirect

Journal of Drug Delivery Science and Technology

journal homepage: www.elsevier.com/locate/jddst





Molecularly imprinting polymethacrylamide onto Cu-based metal-organic framework as a pH-sensitive core-shell nanocarrier for potential anti-cancer drug delivery

Hossein Hosseinzadeh, Siamak Javanbakht, Reza Mohammadi

Polymer Research Laboratory, Department of Organic and Biochemistry, Faculty of Chemistry, University of Tabriz, Tabriz, Iran

ARTICLE INFO

Keywords: Molecularly imprinted polymers Metal-organic framework Doxorubicin pH-responsive Drug delivery system

ABSTRACT

Surface molecularly imprinted polymers (MIPs) are an efficient and rapidly advancing approach, increasingly being utilized in drug delivery systems (DDSs). This research involved synthesizing a core-shell structure, consisting of a metal-organic framework (MOF) core and a doxorubicin (DOX) imprinted polymethacrylamide shell, prepared via precipitation polymerization method in green media. The resulting MOF@MIP was utilized as a nanocarrier for DOX delivery, exhibiting high drug loading capacity and pH responsiveness delivery. The materials were characterized using different techniques such as X-ray diffraction (XRD), scanning electron microscopy (SEM), fourier transform infrared (FTIR), transmission electron microscopy (TEM), dynamic light scattering (DLS), thermal gravimetric analysis (TGA), and zeta potential (ZP). In vitro studies on DOX loading and release demonstrated that a higher amount of DOX was released in a sustained manner under tumor tissue conditions (pH 5, 41 °C) compared to normal physiological conditions (pH 7.4, 37 °C). Additionally, cytotoxicity evaluations revealed significant cytotoxic effects of DOX-loaded MOF@MIP on MCF-7 cells (IC50: 2 μ g/mL). Based on these findings, the synthesized MOF@MIP shows promise as a potential candidate for the development of anticancer therapeutic delivery platforms.

1. Introduction

Cancer is a disease that leads to a considerable amount of deaths each year. Therefore, medical and scientific communities have faced several challenges, which have prompted ongoing attempts to better understand and treat the illness. Chemotherapy stands as a method employed in the treatment of cancer [1,2]. The various challenges exist in this approach, including minimizing the adverse effects of medications on healthy tissues, the precise targeting of drugs to cancerous tissues, the controlled release of drugs within the body, and other related challenges [3,4]. Nanotechnology is considered an advancing field utilized in various medical fields. Nanoscale fillers and particles, which consist of organic and inorganic materials, possess unique chemical, physical, and biological properties that are widely discussed as bioplatforms [5,6]. The utilization of nanoparticles (NPs) in bioscience and biotechnology has shown significant promise in various biological and medical fields, such as gene/drug delivery [7], bioimaging [8], chemotherapy [9], biosensing [8], and photothermal therapy [10]. The use of nanocarriers provides a suitable foundation for engagement in both diagnostics and

therapy, which represent a growing trend in medical practice [11].

Recent studies have focused more on molecularly imprinted polymers (MIPs) and their utilization in biomedical nanoplatforms. Molecular imprinting is an increasingly popular and effective technique for creating highly specific binding sites within a polymeric matrix for molecular recognition [12,13]. The key challenge lies in developing compatible binding sites within polymeric materials that match the template molecules in terms of both shape and chemical functionality. MIPs have been predominantly utilized in various fields such as detection [14], purification [15], and drug delivery [16,17] due to their advantageous characteristics including easy preparation, high selectivity, and stability. These polymers serve as promising platforms in the production of DDSs as they can improve release profiles by prolonging release time and enhancing drug efficiency [18]. The structured interactions between the recognition sites and template (drug) lead to a sustained and controlled drug release mechanism. Moreover, these polymers can release drugs in a feedback-controlled manner, which could be highly beneficial in modern pharmacotherapy for delivering the appropriate medication to a specific patient at the right time and

E-mail address: r.mohammadi@tabrizu.ac.ir (R. Mohammadi).

 $^{^{\}ast}$ Corresponding author.

location [19].

Metal-organic frameworks (MOFs), also referred to as porous coordination polymers, have been extensively researched for a variety of purposes including catalysis, membranes, gas storage, and sensors due to their significant porosities and surface area/volume ratios [20]. Recently, there has been a growing interest in the biomedical applications of MOFs for drug delivery [21]. By reducing the size of MOF particles to the nanoscale, these nano-MOFs can serve as effective nanocarriers for transporting agents used in chemotherapy, imaging, photothermal therapy, or photodynamic therapy [22,23]. In comparison to other porous materials, MOFs offer numerous advantages, such as a high surface area and porosity enabling a high loading capacity for therapeutic agents, as well as the ease of adjusting the chemical and physical (e.g., pore size and shape) properties of MOFs through the use of inorganic or organic ligands [24,25].

In this context, creating the most significant and suitable nanocarrier tolerating biocompatible and non-toxic characteristics presents a significant challenge. For example, acrylamide-type monomers have been frequently utilized in the fabrication of MIPs for the development of pHresponsive DDSs [26–28]. There exist various investigations regarding the development of polyacrylamide-based MIPs for drug delivery purposes [29,30]. However, the investigation into MIPs utilizing methacrylamide (MAm) biocompatible nanoparticles as the shell and MOFs as the core has not been documented in the existing research as far as we know. Polymethacrylamide (PMAm), a widely used and extensively studied polymer, exhibits significant potential for a variety of biomedical applications such as biosensors and drug delivery systems [31,32]. Functional monomers play a crucial role in determining binding interactions in molecular imprinting technology [33]. The presence of an amid (-CONH2) functional group within the molecular structure of PMAm in every repeating unit contributes to its binding with template molecules (i.e., bioactive molecules) following the polymerization process [29,30]. The presence of a methyl functional group in PMAm, in comparison to polyacrylamide, influences the rigidity of a MIP, and its affinity for efficient binding sites [34]. Furthermore, the presence of a metal-organic framework as a core in the nanocomposite, owing to its porous characteristics, enhances the capacity for drug loading and contributes to a controlled release mechanism.

Based on our previous investigation of MIPs [35–37], herein, this study aims to create a pH-responsive nanocarrier through a more effective drug imprinting technique by combining MOF and MIP. On the other hand, this research deals with the fabrication of MOF@MIPs for imprinting the anticancer DOX drug, commonly used in chemotherapy. The exclusive features of the resulting MOF@MIP such as pH sensitivity, increased capability for drug loading, and controlled/targeted drug delivery make the designed nanocomposite for potential smart drug release system.

2. Material and methods

2.1. Materials

Methacrylamide (MAm), N,N-Methylenebisacrylamide (MBA), Dimethylformamide (DMF, 99.8 %), Ammonium persulfate (98 %, APS), Copper (II) nitrate trihydrate (Cu(NO3).3H2O), Terephthalic acid (H2BDC, 98 %), Hydroxyethylmethacrylate (HEMA), N,N'-dicyclohexylcarbodiimide (DCC) and Pyridine were purchased from Sigma-Aldrich Co. Doxorubicin hydrochloride (DOX) was obtained from Sobhan Pharmaceuticals (Iran). All of the components listed above and all the solvents employed in the experiments were of analytical grade and were utilized without undergoing additional purification. Deionized water was generated through the utilization of a Milli-Q system. (Millipore, Milford, MA, USA).

2.2. Characterization

UV–Vis spectrophotometer (Shimadzu, Model 1700) was used to determine the UV–Vis spectra. An FT-IR spectrometer (Bruker Instruments, model Aquinox 55, Germany) with a scanning range of 400–4000 cm⁻¹ was used to record the Fourier transform infrared (FT-IR) spectra. The instrument used for the thermogravimetric analysis (TGA) was LINSEIS STA PT-1000 Germany. The samples' crystalline phase analyses were determined by X-ray diffraction (XRD) measurement (Siemens, D500 with Cu-Ka radiation at 35 Kv). A scanning electron microscope (SEM, SEM-TESCAN MIRA3-FEG) and Transmission Electron Microscopy (TEM, TEM Philips EM 208S) were used to examine the surface morphology of the samples. Zeta potential (ZP) and dynamic light scattering (DLS) measurements were performed using a DLS-ZP/particle sizer (Malvern model MAL1032660).

2.3. Synthesize of Cu-MOF

Cu-MOF was synthesized by precipitation method [38,39]. Briefly, 1.453 mmol (351 mg) of Cu(NO₃).3H₂O and 1.453 mmol (241 mg) of H₂BDC dissolved in 50 mL of DMF. The resulting mixture was ultrasonicated for 10 min to obtain a homogenous mixture. The final solution was heated at 125 °C for 24 h under constant stirring. After the reaction was completed, the products were collected by centrifugation, and they were then washed twice with chloroform and DMF, respectively, then overnight dried at 60 °C.

2.4. Synthesis of Cu-MOF/HEMA

The HEMA-functionalized Cu-MOF was synthesized through a modified Steglich esterification method [40]. First, 500 mg of synthesized MOF was dispersed in 100 mL of DMF and sonicated until became the homogenous solution. Then, 200 mg of DCC and 100 mg of HEMA and Pyridine as a catalyst were added to the above mixture. The final solution was heated at 70 $^{\circ}$ C for 24 h at a dark place under a nitrogen atmosphere and constant stirring. Finally, the precipitate was collected by centrifuging and washed with DMF and Ethanol, respectively, and dried at 40 $^{\circ}$ C.

2.5. Synthesize of MOF@MIP and MOF@NIP

The core-shell nanocomposite was produced by the free-radical polymerization method using MOF as a core, DOX as a template, MAm as a functional monomer, MBA as a cross-linker, and APS as an initiator [35]. Briefly, 100 mg of synthesized Cu-MOF/HEMA was dispersed in 50 mL of bi-distilled water. After that 1 mmol (543 mg) of DOX, 2 mmol (175 mg) of MAm, 8 mmol (1250 mg) of MBA, and 0.2 mmol (60 mg) of APS were added to the above solution and were heated at 60 °C for 24 h under constant stirring $\rm N_2$ atmosphere in a dark place. After completing the reaction, the precipitate was collected by centrifuging then washed with ethanol three times and dried at 40 °C. The procedure mentioned above was also used to synthesize MOF@NIP as a control sample without the using template molecule, DOX.

2.6. Binding studied

The binding study was performed in bidistilled water. In summary, 10 mg of MOF@MIP and MOF@NIP were dissolved in 10 mL of various DOX solution concentrations (10–1000 ppm). The prepared solutions were stored in a dark place and shaken at room temperature for 24 h. After centrifuging for 15 min, the supernatant of precipitation was separated and used to calculate the concentration of DOX. The binding capacity of MOF@MIP and MOF@NIP were determined by Q (mg $_{\rm drug}/g$ $_{\rm nanocarrier}$) as the following Eq. (1):

Table 1
DOX release kinetics.

Kinetics model Zero-order	Coefficient of determination (R ²) MOF@MIP MOF@NIP			
	0.528	0.347	0.282	0.264
	First-order	0.526	0.346	0.265
Higuchi	0.699	0.537	0.465	0.439
Weibull	0.998	0.981	0.996	0.998

$$Q = \frac{(C0 - Ce) * V}{m} \tag{1}$$

2.7. DOX loading

Generally, 50 mg of MOF@MIP and MOF@NIP were added to 50 mL of 1000 ppm concentration of DOX and shaken continuously for 48 h at room temperature in the dark tube. After the separation of the precipitate by centrifuging, the sample was washed with deionized water to eliminate the unlocated drugs. UV–vis spectroscopy was used to determine the amount of loaded DOX using the standard DOX calibration curve. The loading efficiency (LE) and loading capacity (LC) were estimated with Eq. (2), and Eq. (3), respectively.

$$\% LE = \frac{\text{Mass of drug in nanocarrier}}{\text{Mass of drug fed inotially}} *100$$
 (2)

$$\%LC = \frac{\text{Mass of drug in nanocarrier}}{\text{Mass of nanocarrier}} *100$$
 (3)

2.8. In vitro DOX release studies

The in vitro DOX release behavior from nanocarrier was studied in two different pH conditions (i.e., pH 5 and 7.4). Generally, 10 mg of each nanocarrier was immersed in 10 mL of PBS buffer solution in a simulated tumor tissue (pH 5, 41 $^{\circ}$ C) environment and physiological conditions (pH 7.4, 37 $^{\circ}$ C). At specific time intervals, sufficient volume was collected from the releasing media, and the same amount of new medium was replaced. The UV–Vis spectrophotometer was used for calculating the amount of DOX released from the nanocarrier. Eq. (4) was used for calculating the percentage of released DOX.

Drug release =
$$\frac{\text{The amount of released drug}_*}{\text{The amount of loaded drug}} 100$$
 (4)

2.9. Drug release kinetics

By using mathematical models such as the zero-order (Eq. (5)), first-order (Eq. (6)), Higuchi (Eq. (7)), and Weibull models (Eq. (8)) to analyze the release data, the release mechanism of the DOX from nanocarrier was examined by Mathcad version 15 software [41,42]. The results are reported in Table 1.

$$F = K0 t ag{5}$$

$$Ln(1-F) = -Kf t (6)$$

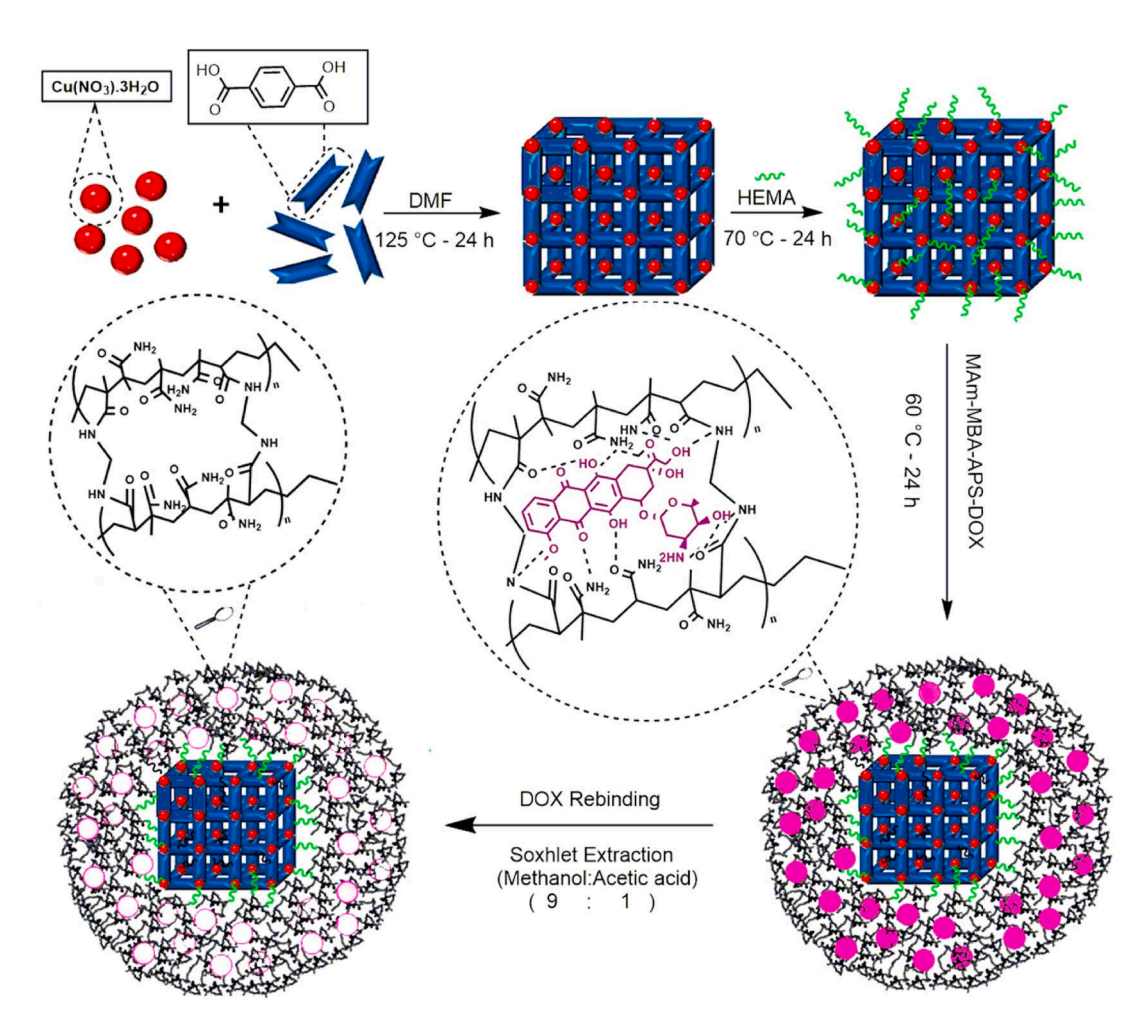


Fig. 1. The schematic of synthesizing MOF@MIP nanocarrier and DOX rebinding.

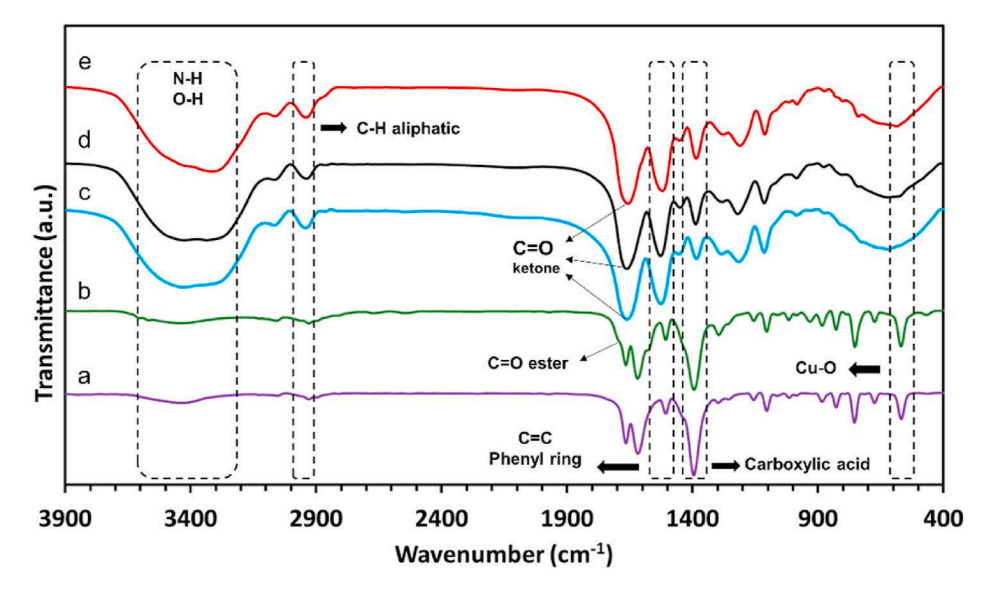


Fig. 2. The FT-IR spectra of a) Cu-(BDC), b) Cu-MOF/HEMA, c) MOF@NIP, d) DOX-loaded MOF@MIP, e) MOF@MIP.

$$F = Kh t^{1/2} \tag{7}$$

$$Ln[-\ln(1-F)] = -\beta \ln td + \beta \ln t$$
(8)

where K_0 , K_f , K_h , β , t_d , and F describe the constant of drug release for the zero-order model, the constant of first-order drug release, Higuchi's dissolution constant, the shape parameter, the time scale of the process, and drug release rate at time t, respectively.

2.10. MTT measurement

MTT tests were employed to assess the in vitro cytotoxicity of the synthesized materials [43]. Typically, MCF-7 cells were chosen and placed in 96 well plates at a density of 6000 cells per well in 200 μL of cell medium and incubated for a period of 24 h. The resulting cells were exposed to DOX, DOX-loaded MOF@MIP, and DOX-loaded MOF@NIP with an equivalent drug concentration. The equal concentration of DOX was adjusted (from 0.5 to 8 μg/mL) by considering its release profile of nanocarriers. Furthermore, the cells were treated with blank NPs (MOF@MIP and MOF@NIP) to assess the cytocompatibility of the samples. Following 48 h incubation period, cell cytotoxicity was assessed by removing the culture medium from each well and adding 50 μL of MTT solution with a concentration of 3 mg/mL to the 100 μL of fresh culture medium in each well. After discarding the culture medium and incubating for 4 h at 37 $^{\circ}\text{C},$ dimethyl sulfoxide (DMSO) in a volume of $100~\mu L$ was added to solubilize the formazan crystals. The cell count was determined using a hemacytometer (DANA-DA3200). The experiments were conducted in triplicate for every sample.

2.11. Statistical analysis

The mean \pm standard deviation was employed to present the outcomes. To determine statistical significance, a one-way analysis of variance (ANOVA) was conducted using the Microsoft Excel software, while considering a P value below 0.05. Each experiment was repeated a minimum of three times.

2.12. DAPI staining

DAPI staining was employed to identify nuclear condensation and fragmentation in apoptotic cells, which were triggered by the control, DOX/MOF@MIP, and DOX/MOF@NIP samples. MCF-7 cells (5 \times 10⁵

cells/well) were cultivated on glass coverslips and subjected to the samples at their IC50 concentrations for a duration of 48 h. After the treatment, the cells were rinsed, fixed with paraformaldehyde, permeabilized with Triton X-100, stained with DAPI, and apoptosis was assessed through fluorescence microscopy. All experimental procedures were conducted in triplicate.

2.13. Annexin V staining apoptosis analysis

The evaluation of apoptosis-mediated cytotoxicity in neoplastic cells was conducted employing an Annexin V/PI dual staining assay, adhering strictly to the protocols outlined by the manufacturer (Invitrogen, USA). MCF-7 cells (3 \times 10 5 cells/well) were cultivated in 6-well plates and maintained in a controlled environment at 37 $^{\circ}\text{C}$ with 5 % CO2 overnight. The cells underwent treatment conditions (control, DOX/MOF@MIP, and DOX/MOF@NIP) at their respective IC50 concentrations. Following the treatment period, the cells were detached, washed with ice-cold PBS, and subjected to centrifugation at 4000 rpm for 5 min. Thereafter, 5 μL of Annexin V-FITC and 5 μL of propidium iodide (PI) staining solution were introduced into the cell suspension, and the resultant mixture was incubated in the dark for 5 min at 25 $^{\circ}\text{C}$. Subsequently, flow cytometry analysis was executed utilizing an Annexin V-FITC apoptosis detection kit (Ebioscience, USA) on a FACS Calibur flow cytometer (USA).

3. Result and discussion

3.1. Synthesis of MOF@MIP

Fig. 1 illustrates the synthesis scheme of the MOF@MIP nanocarrier by precipitation free-radical polymerization method [35]. First, the Cu-MOF was prepared via a precipitation technique; subsequently, the MOF was modified by HEMA via an esterification method to produce functionalized MOF. In the next stage, the MOF@MIP nanocarrier was synthesized utilizing a functionalized Cu-MOF as core, MAm as the functional monomer, MBA as the cross-linker, and DOX as a template through a free-radical polymerization process. During this procedure, DOX reacted with the functional monomers of MIP via H-bonding interactions (Fig. 1). Finally, the DOX was eliminated by employing the "Soxhlet apparatus" technique, establishing recognition sites for the template molecule. It should be mentioned that using unfunctionalized Cu-MOF in the synthesis of MOF@MIP nanocarrier results in two phase materials in reaction media, the first one is MOF, and the other is MIP.

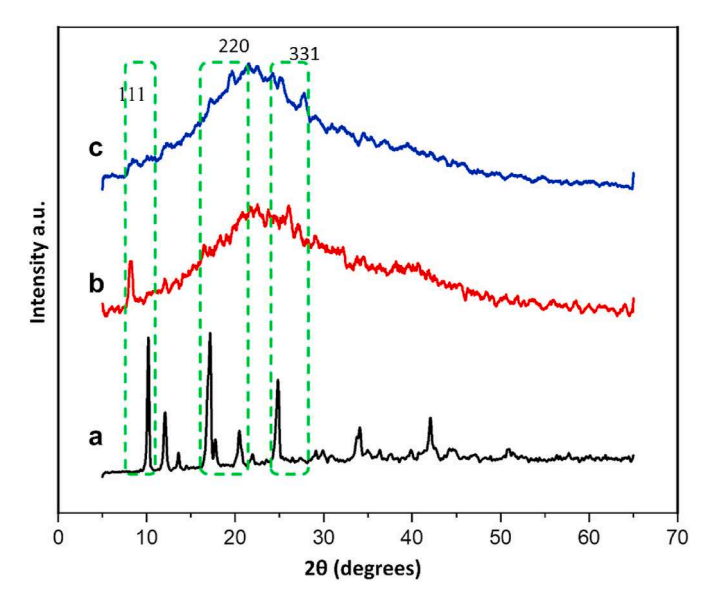


Fig. 3. XRD spectra for a) Cu-MOF/HEMA, b) MOF@MIP, c) MOF@NIP

This revealed the functionalizing Cu-MOF with HEMA is necessary for successful surface imprinting of MIP onto Cu-MOF.

3.2. FT-IR analysis

The FT-IR spectra of the Cu-(BDC), Cu-MOF/HEMA, MOF@NIP, MOF@MIP, and DOX-loaded MOF@MIP are shown in Fig. 2. The observed peaks at 468 and 569 cm⁻¹ are associated with the stretching vibration of the Cu-O bond. The peaks that appeared in 1619 and 1394 cm⁻¹ in all samples are associated to the asymmetric and symmetric stretching of the carboxylate groups in cross-linker, respectively [44]. In the HEMA-functionalize spectra, the peak emerged at 1666 cm⁻¹ is related to the C=O bond of the ester group, proving the successful functionalizing Cu-(BDC) with HEMA [35]. In the prepared MOF@MIP and MOF@NIP nanocomposite, the absorption peaks at 1522, 1660 and 2943 cm⁻¹ corresponded to phenyl rings, C=O bonds, and aliphatic C-H bonds, respectively. Furthermore, the tensile vibration peak of the hydroxyl group overlaps with the absorption peak of the N-H group in MAm and MBA, which is approximately appeared around 3400 cm⁻¹ [37]. Moreover, due to the overlapping C-H bending with Cu-O stretching vibrations, the related peak was disappeared in the other spectrums. The presence of these bonds revealed the successful synthesis of MOF@MIP nanocomposites.

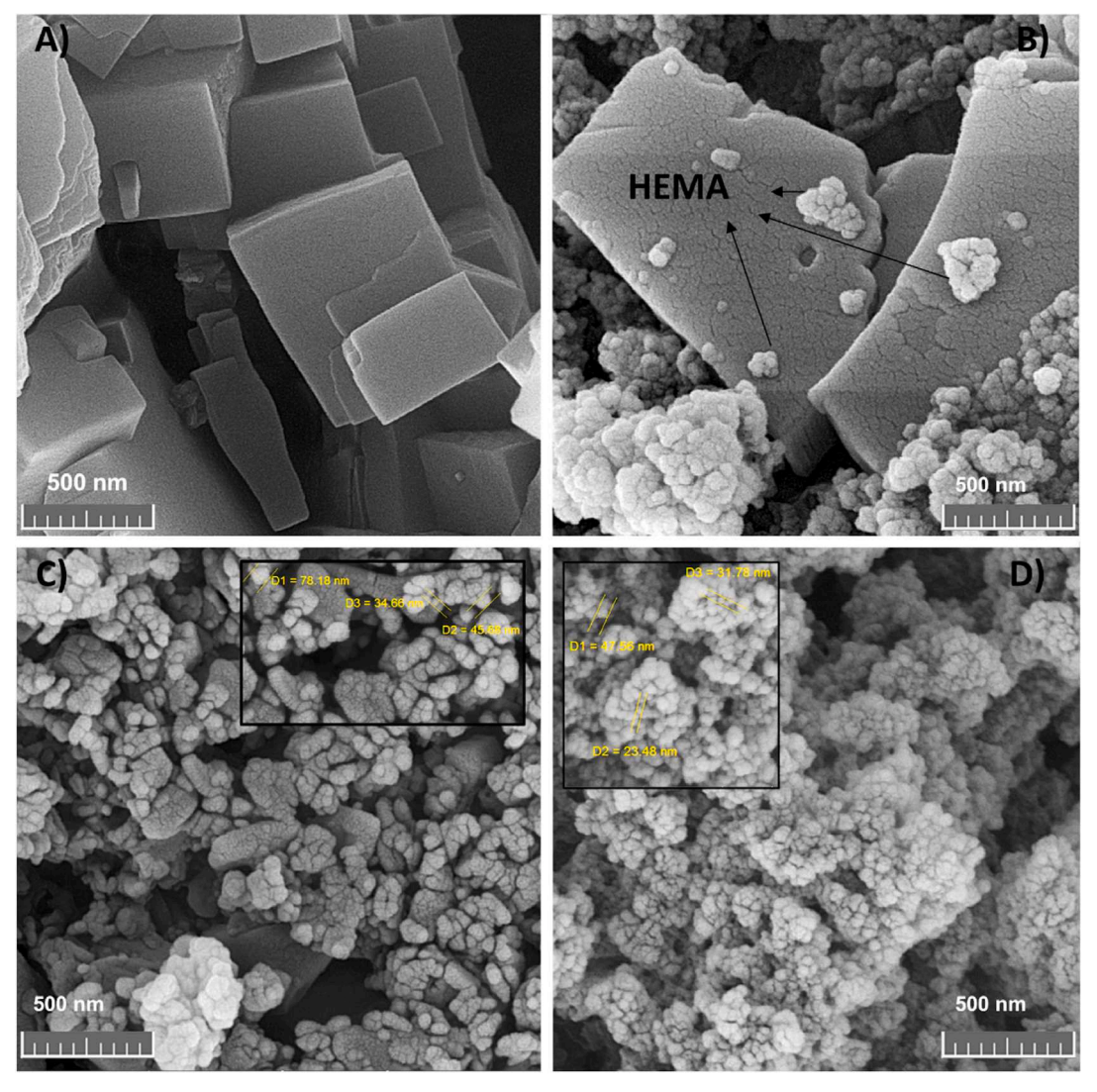


Fig. 4. The SEM image of A) Cu-(BDC), B) Cu-MOF/HEMA, C) MOF@MIP, D) MOF@NIP.

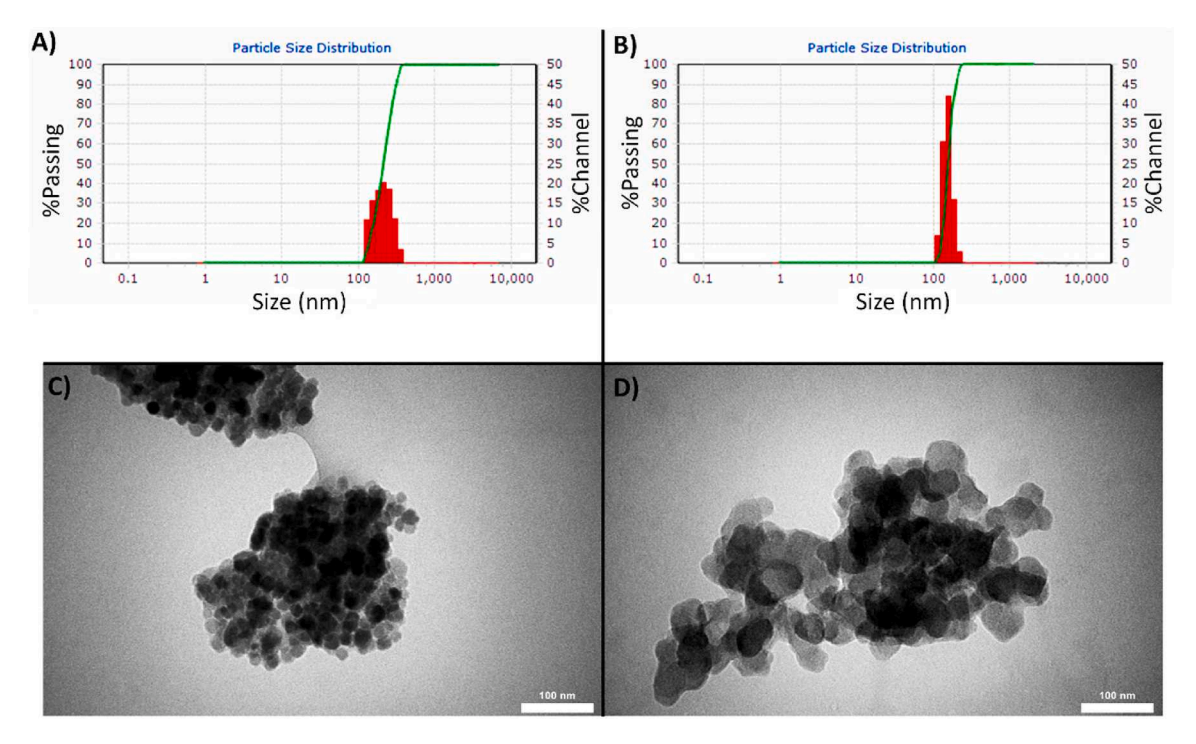


Fig. 5. The particle size distributions of A) MOF@MIP, B) MOF@NIP. The TEM image of C, D) MOF@MIP

3.3. XRD analysis

X-ray is a highly effective method for analyzing the crystal properties of synthesized composites. The XRD patterns of Cu-MOF, MOF@MIP and MOF@NIP in the 2θ range of 5–65° are demonstrated in Fig. 3. In the XRD spectra of Cu-MOF, the peaks that appear in $2\theta=10.2^\circ,12.04^\circ,13.64^\circ,17.16^\circ,17.74^\circ,20.42^\circ,24.8^\circ,34.14^\circ$ and 42.12° , corresponded to (111), (200), (202), (220), (311), (222), (313), (331), (402) and (420) planes of Cu-MOF confirmed its FCC cubic crystal structure [45,46]. The broad peak observed at about $2\theta=20$ –25 in the XRD spectra of the MOF@MIP and MOF@NIP nanocomposites can be attributed to the

amorphous nature of the polymer network. Also, the displacement of the peaks shown in the MOF@MIP and MOF@NIP diagrams compared to Cu-MOF can be due to the covering of the crystal structure of the core by the polymer [47]. The reason for the decrease in the intensity of Cu-MOF peaks in MOF@MIP and MOF@NIP can be due to the lower weight ratio of Cu-MOF into the polymeric matrix [37].

3.4. Morphological and DLS analyses

SEM and TEM analyses were used to investigate the morphology of the nanocarrier as shown in Figs. 4 and 5. The SEM images of MOF and

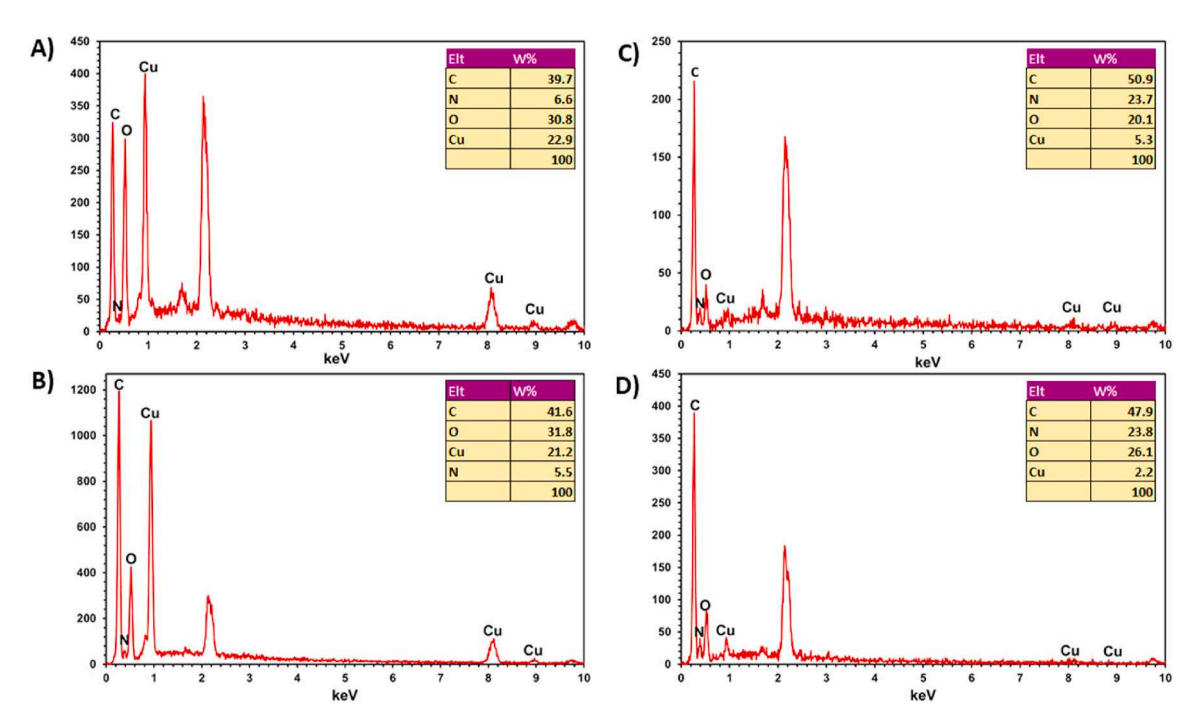


Fig. 6. The EDX analysis of A) Cu-(BDC), B) Cu-MOF/HEMA, C) MOF@MIP, D) MOF@NIP.

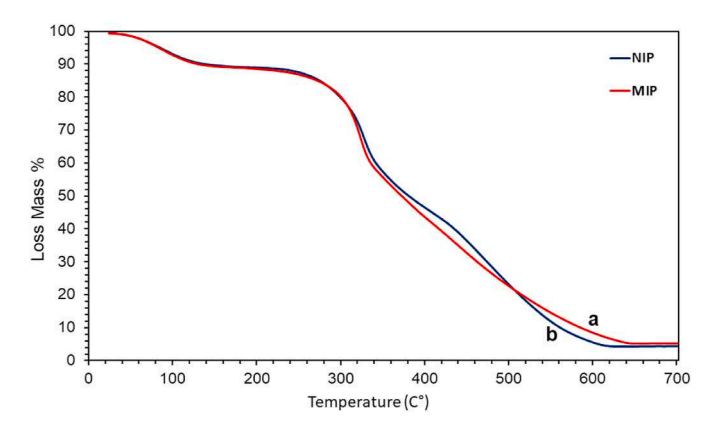


Fig. 7. The TGA of a) MOF@MIP and b) MOF@NIP.

MOF-HEMA show the cubic crystal structure of the synthesized materials, which is also consistent with the XRD analysis. In addition, according to the SEM image of MOF-HEMA, the presence of spherical particles on the surface of MOF can be related to the functionalizing MOF with HEMA. Also, this revealed that the functionalization of MOF with HEMA has not changed its crystalline morphology [48]. SEM and TEM images of MOF@MIP and MOF@NIP showed spherical structures with irregular surface morphology (about 60 nm) due to the grafted polymer (Fig. 4). In addition, it showed little differences in the morphologies of MOF@MIP and MOF@NIP, demonstrating the polymerization process is not considerably affected by the addition of template in the reaction medium. Besides, TEM images of MOF@MIP revealed the characteristic core-shell structure, wherein the inner MOF cores are encapsulated by an amorphous polymeric layer [49].

Particle size distribution was obtained by the DLS technique (Fig. 5). According to the diagram, the average particle size for MOF@MIP and MOF@NIP was calculated to be about 150 and 130 nm, respectively. The

size difference between MIP and NIP particles can be due to the presence of DOX drugs in the MIP structure, which increases the size of the particles [50]. Also, the difference in particle size between DLS and SEM analysis can be due to the slight swelling of particles in water over the performing DLS analysis. Moreover, in deionized water, the average zeta potentials of the MOF@MIP and MOF@NIP were determined to be +14.4 and +11.9 mV respectively. Additionally, the PDI of nanocarriers were calculated at about 6.39 and 11.35 for MOF@MIP and MOF@NIP, respectively. The positive charge of prepared nanocomposites can be due to the large number of amide moieties in their structures [51]. The greater charge value of the MOF@MIP compared to the MOF@NIP can be related to the quantity of DOX that is still present even after the removal of the template [35]. The positive charge of particles can be considered a good factor in nanocarrier. This is because of the negative surface charge of cancer cells, causing better absorption of the composite into the cells, enhancing the efficiency and performance of the nanocarrier [52].

3.5. EDX analyses

The EDX analysis of the synthesized samples is shown in Fig. 6. In general, the analysis of EDX is performed to illustrate the various elements present on the surface of materials. The obtained results emphasize the presence of C, O, Cu, and N elements. Furthermore, the percentage of elements present on the surface of samples is related to the peak intensity of the element. According to the obtained results, the higher percentage of C and O elements in the HEMA-functionalized Cu-MOF than that of the Cu-MOF confirms the successful functionalization of MOF with HEMA. In addition, according to the percentage of elements obtained from MOF@MIP and MOF@NIP nanocomposites, it can be concluded that the difference in the percentage of elements in these structures compared to the MOF and MOF-HEMA, can be due to the presence of C, O, and N in the structure of MAm and cross-linker (MBA), which confirms the successful polymerization [53].

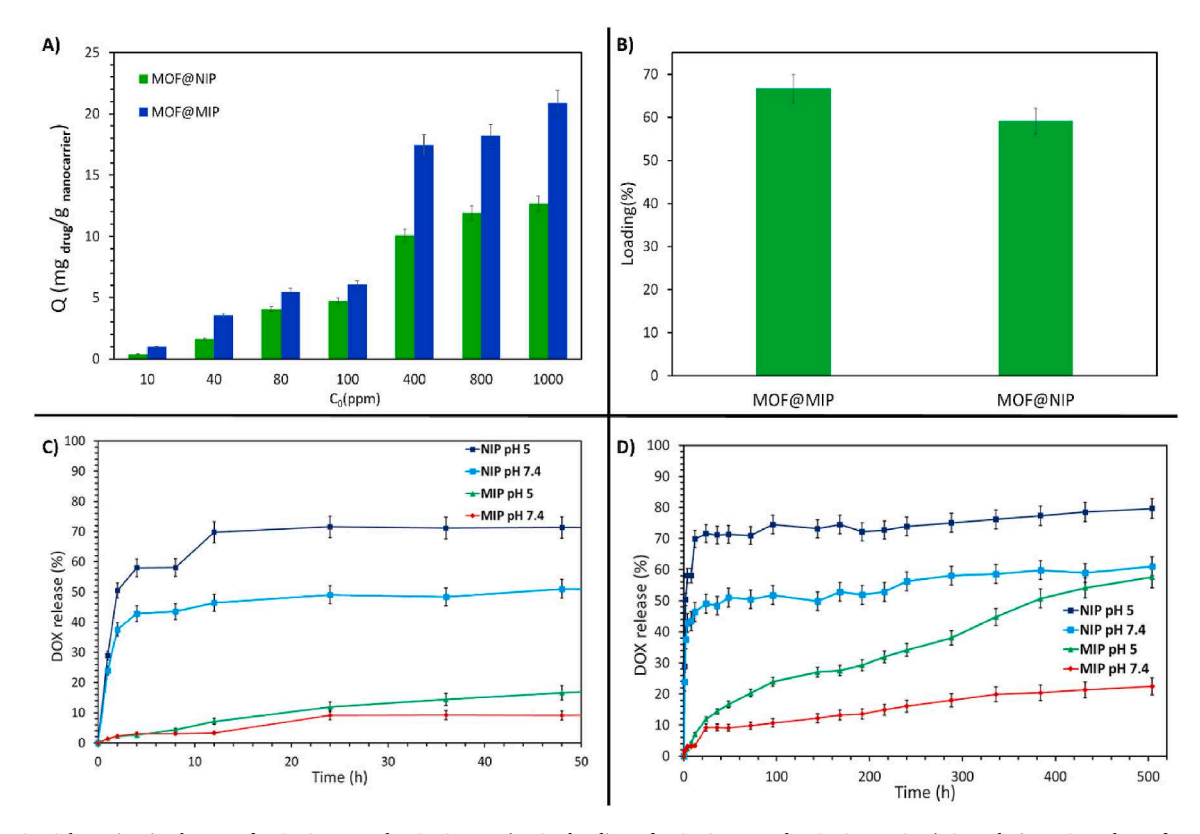


Fig. 8. A) DOX Adsorption isotherms of MOF@MIP and MOF@NIP. B) DOX loading of MOF@MIP and MOF@NIP. C, D) Cumulative DOX release from MOF@MIP and MOF@NIP at different pH (P < 0.05).

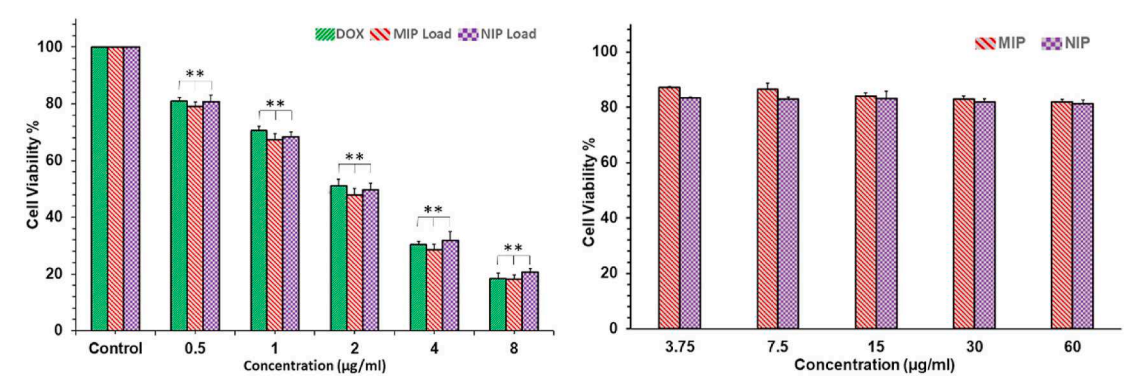


Fig. 9. The MTT results of MCF-7 cells after 48 h incubation time with various concentrations of DOX, nanocarrier, and DOX-loaded MOF@MIP and MOF@NIP (**P < 0.05).

3.6. TGA analyses

TGA was utilized to investigate the thermal stability of MOF@MIP and MOF@NIP nanocomposites, and the findings are illustrated in Fig. 7. As seen in the TGA curve, the weight loss process was observed in three stages at the temperature range of 20–700 $^{\circ}$ C. The initial reduction in weight, measuring approximately 8.84 % for MOF@MIP and 9 % for MOF@NIP, occurred within the temperature range of 24-123 °C. This decrease in weight can be ascribed to the elimination of moisture that had been absorbed by the samples [54]. The second weight reduction occurred at approximately 85.26 and 84 % between temperatures of 125–643 °C can be ascribed to the degradation of the polymer network and carbon skeletal present on the surface of the MOF core in both MOF@MIP and MOF@NIP, respectively. Finally, a weighted residual of approximately 7 % was observed at 700 °C, likely due to the presence of Cu metal available in MOF structure remnants following the burning process [55]. The minimal residual mass in the TGA diagrams compared to the reported pure Cu-(BDC) in previous work [56] can be due to the degradation of the polymeric network in the nanocomposite structure.

3.7. Binding kinetics

The static adsorption experiments were investigated to assess the binding capacity of the MOF@MIP and MOF@NIP. Fig. 8 illustrates the DOX binding capacity to MOF@MIP and MOF@NIP. As seen in Fig. 8, the amount of DOX binding capacity to nanocomposites was increased by increasing the initial concentration of DOX. In the various concentrations of DOX, the capacity of MOF@MIP for DOX adsorption was higher than that of the MOF@NIPs. This is because the MOF@MIP has both specific and nonspecific binding sites, whereas the MOF@NIP exclusively possesses nonspecific binding sites [33,35]. Both noncovalent and H-bonding interactions may serve as potential adsorption mechanisms for DOX on the nanocomposite structure [37]. For this reason, these nanocomposites can release drugs slowly at the right time and in the right place in modern classes of drug delivery.

3.8. Drug loading and release studies

The amount of loading DOX in the MOF@MIP and MOF@NIP nanocomposites was calculated to be 66.64 % and 59.1 %, respectively (Fig. 8). As well, the loading capacity for the MOF@MIP and MOF@NIP were calculated 1.33 % and 1.18 % respectively. The higher amount of drug loaded in MOF@MIP than in MOF@NIP was due to the presence of drug recognition sites and specific cavities in the MIP structure [37]. Fig. 8 shows the cumulative release profiles of DOX from MOF@MIP and MOF@NIP structures at pH 7.4 and 5. According to the graphs, it can be seen that a pH-responsive property and the most of drug releases occur in acidic conditions (pH 5, conditions of the cancer environment). Whereas the rate of drug release from the MOF@MIP is slower than

MOF@NIP, it showed a sustained and more controlled release. This can be due to more specific cavities and interactions between the drug and polymer matrix [57,58]. Furthermore, it was noted that the rate of drug release from the nanocomposites at pH 5 was more than the pH 7.4 (physiological conditions of the body). At pH 7.4, the H-bonding between the functional groups of the polymer matrix and the NH and OH groups of the DOX are stable. While, at pH 5, protonation of the DOX amino groups causes the loss of H-bonding and increases the drug's solubility and hydrophilicity [35], additionally, due to the lack of stability and degradation of Cu-MOF used in an acidic environment, the cancer tissues (acidic environment) cause the degradation of the nanocarrier's structure [59,60]; therefore, DOX is rapidly released in an acidic medium. Furthermore, an analysis of the release Kinetic of DOX showed that the Weibull model is the most suitable model for the MOF@MIP at pH of 5 (Table 1). In the Weibull model, the predominant mechanisms of release are solvent diffusion and polymer chain relaxation, while polymer swelling represents a less significant mechanism contributing to a sustained and regulated release rate [61]. The parameter β is crucial for defining the characteristics of the release curve. A β value of 1.0 is associated with an exponential release profile, β values exceeding 1.0 signify a sigmoidal profile, whereas β values below 1.0 indicate a parabolic curve [62,63]. In this research, the β values obtained were primarily below 1.0, with an average value of 1.53. These values are indicative of the general morphology of the release profiles observed in the MOF@MIP nanocarrier. The results recommended the designed nanocarrier as a good candidate for anti-cancer DDSs.

3.9. Cytotoxicity study

The cytotoxicity of the synthesized nanocarrier was estimated by using the MTT test. As shown in Fig. 9, the cytotoxicity against MCF-7 cells showed a dose- and time-dependent behavior, in which longer incubations at higher active drug concentrations lead to high cytotoxicity. At the equal concentration of DOX, the DOX-loaded MOF@MIP nanocomposite was more cytotoxic than both free DOX and DOX-loaded MOF@NIP. The IC50 value for DOX-loaded MOF@MIP was calculated to be about 2 μ g/mL for 48 h of incubation time. The elevated cytotoxicity observed in DOX-loaded MOF@MIP is probably attributed to the positively charged nanocarrier and the existence of amide bonds in the structure of the employed MAm and MBA, forming pseudo peptide skeletons in the nanocarrier. It makes a strong affinity in nanocarriers for nucleic acids and cells, as well as it may speed up their interactions with cells and tissues after entering [35,64,65]. In addition, the nanoscale size of the synthesized nanocomposite facilitated the penetration into the cancerous tissues and enhanced the cytotoxicity of the drug [66]. Remarkably, the blank nanocarriers demonstrated cytocompatibility behavior as the cell viability maintained above 80 % after 48 h of incubation. According to the results, the prepared MOF@MIP nanocarrier could be a good candidate for anticancer DDSs.

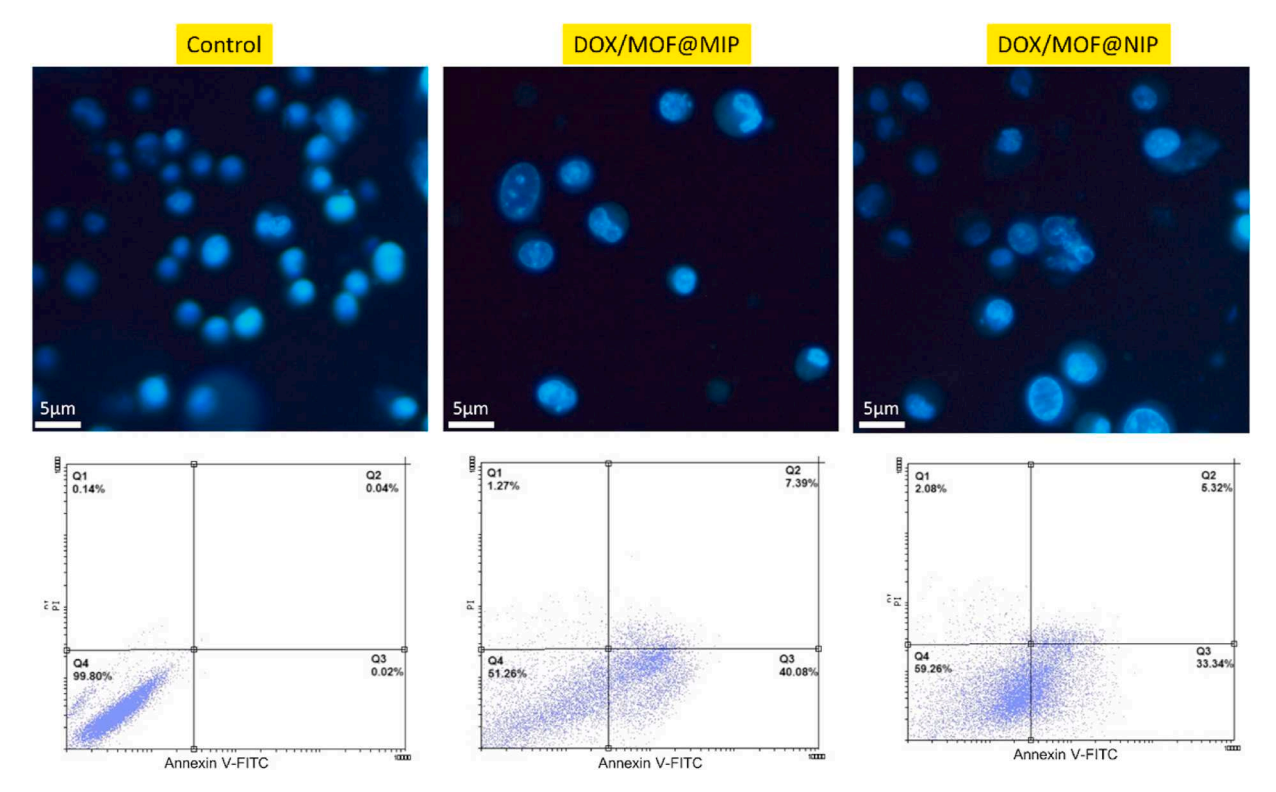


Fig. 10. Apoptosis study by DAPI staining and flow-cytometry after treatment of MCF-7 cells with DOX-loaded MOF@MIP and MOF@NIP.

3.10. Apoptosis studies

To further assess the outcomes derived from the MTT assay, a fluorescence imaging experiment was performed on MCF-7 cells undergoing various treatments (Fig. 10). DAPI staining, a reliable technique for discerning cellular apoptosis and necrosis predicated on its affinity for binding to cellular nuclei, was employed in conjunction with fluorescence imaging techniques. To end this, MCF-7 cells were subjected to treatments with DOX-loaded MOF@MIP, and MOF@NIP. Cells that received treatment with DOX-loaded MOF@MIP demonstrated a marked reduction in viability when compared to the control group and MOF@NIP, accompanied by an increase in blue fluorescence indicative of nuclear fragmentation and chromatin condensation [67]. This phenomenon revealed that DOX was improvly transported into the tumor cells using the prepared MOF@NIP nanocarriers, facilitating circumvent multidrug resistance (MDR) efflux, known as "stealth" endocytosis [35]. Moreover, flow cytometric analysis was utilized to quantify the apoptotic rate of MCF-7 cells. The treatment with DOX/MOF@MIP displays significantly increased apoptotic cell numbers (~49 %) compared to DOX/MOF@NIP and control (Fig. 10). This indicates that the expression of DOX/MOF@MIP is accompanied by cell apoptotic evolution [68].

4. Conclusion

In brief, the molecularly imprinted method was utilized to produce a DOX imprinted PMAm using Cu-MOF NPs as the pH-responsive anticancer drug carrier. Initially, Cu-MOF NPs were synthesized and then modified with HEMA. In the next step, by using MAm as a monomer, MBA as a crosslinker, and DOX as template molecules the MOF@MIP nanocomposite was synthesized by free-radical polymerization. Different methods were employed to analyze the synthesized materials, confirming the effectiveness of the current approach. Binding tests demonstrated the presence of specific recognition sites in the MOF@MIP than MOF@NIP. The in vitro drug release profile displayed minimal drug leakage in physiological conditions (pH 7.4, 37 °C) from

MOF@MIP, reducing potential side effects. Conversely, drug release at tumor conditions (pH 5, 41 $^{\circ}$ C) showed a sustained increase, leading to desired cytotoxicity against cancer tissues. Significantly, MTT assay results indicated the cytotoxicity of DOX-loaded MOF@MIP towards MCF-7 cells, while blank MOF@MIP exhibited good cytocompatibility. These findings suggest that the synthesized MOF@MIP could serve as an effective nanocarrier for targeted anticancer drug delivery due to its pH-responsive nature.

CRediT authorship contribution statement

Hossein Hosseinzadeh: Writing – original draft, Visualization, Software, Methodology, Investigation, Formal analysis, Data curation, Conceptualization. Siamak Javanbakht: Writing – review & editing, Validation, Project administration. Reza Mohammadi: Writing – review & editing, Validation, Supervision, Resources.

Availability of data and materials

The data that support the findings of this study are available from the corresponding author, upon reasonable request.

Declaration of competing interest

The authors declare that they have no known competing financial interests or personal relationships that could have appeared to influence the work reported in this paper.

Acknowledgments

This research was supported with a research grant of the University of Tabriz (number SAD/2389–14020820).

Data availability

Data will be made available on request.

References

- V.T. DeVita Jr., E. Chu, A history of cancer chemotherapy, Cancer Res. 68 (21) (2008) 8643–8653.
- [2] M. Hassan, J. Ansari, D. Spooner, S. Hussain, Chemotherapy for breast cancer, Oncol. Rep. 24 (5) (2010) 1121–1131.
- [3] S.W. Fatima, S.K. Khare, Benefits and challenges of antibody drug conjugates as novel form of chemotherapy, J. Contr. Release 341 (2022) 555–565.
- [4] S. Senapati, A.K. Mahanta, S. Kumar, P. Maiti, Controlled drug delivery vehicles for cancer treatment and their performance, Signal Transduct. Targeted Ther. 3 (1) (2018) 7
- [5] P.G. Falireas, M. Vamvakaki, Triple-responsive block copolymer micelles with synergistic pH and temperature response, Macromolecules 51 (17) (2018) 6848–6858.
- [6] S. Javanbakht, A. Shaabani, Multicomponent reactions-based modified/ functionalized materials in the biomedical platforms, ACS Appl. Bio Mater. 3 (1) (2019) 156–174.
- [7] R. Kurapati, T.W. Groth, A.M. Raichur, Recent developments in layer-by-layer technique for drug delivery applications, ACS Appl. Bio Mater. 2 (12) (2019) 5512–5527
- [8] K.-S. Kim, J.-H. Han, J.-H. Park, H.-K. Kim, S.H. Choi, G.R. Kim, H. Song, H.J. An, D.K. Han, W. Park, Multifunctional nanoparticles for genetic engineering and bioimaging of natural killer (NK) cell therapeutics, Biomaterials 221 (2019) 119418.
- [9] R.A. Mustafa, M. Ran, Y. Wang, J. Yan, Y. Zhang, J.M. Rosenholm, H. Zhang, A pH/ temperature responsive nanocomposite for chemo-photothermal synergistic cancer therapy, Smart Materials in Medicine 4 (2023) 199–211.
- [10] Z. Zhou, Y. Yan, L. Wang, Q. Zhang, Y. Cheng, Melanin-like nanoparticles decorated with an autophagy-inducing peptide for efficient targeted photothermal therapy, Biomaterials 203 (2019) 63–72.
- [11] B. Kateb, K. Chiu, K.L. Black, V. Yamamoto, B. Khalsa, J.Y. Ljubimova, H. Ding, R. Patil, J.A. Portilla-Arias, M. Modo, Nanoplatforms for constructing new approaches to cancer treatment, imaging, and drug delivery: what should be the policy? Neuroimage 54 (2011) \$106-\$124.
- [12] J.J. BelBruno, Molecularly imprinted polymers, Chem. Rev. 119 (1) (2018)
- [13] L. Liu, N. Li, M. Chen, H. Yang, Q. Tang, C. Gong, Visible-light-responsive surface molecularly imprinted polymer for acyclovir through chicken skin tissue, ACS Appl. Bio Mater. 1 (3) (2018) 845–852.
- [14] M.J. Whitcombe, I. Chianella, L. Larcombe, S.A. Piletsky, J. Noble, R. Porter, A. Horgan, The rational development of molecularly imprinted polymer-based sensors for protein detection, Chem. Soc. Rev. 40 (3) (2011) 1547–1571.
- [15] L.N. Gómez-Arribas, J.L. Urraca, E. Benito-Pena, M.C. Moreno-Bondi, Tag-specific affinity purification of recombinant proteins by using molecularly imprinted polymers, Anal. Chem. 91 (6) (2019) 4100–4106.
- [16] R. Liu, A. Poma, Advances in molecularly imprinted polymers as drug delivery systems, Molecules 26 (12) (2021) 3589.
- [17] S.A. Zaidi, Molecular imprinted polymers as drug delivery vehicles, Drug Deliv. 23 (7) (2016) 2262–2271.
- [18] D. Cunliffe, A. Kirby, C. Alexander, Molecularly imprinted drug delivery systems, Adv. Drug Deliv. Rev. 57 (12) (2005) 1836–1853.
- [19] P. Lulinski, Molecularly imprinted polymers as the future drug delivery devices, Acta Pol. Pharm. 70 (2013) 601–609.
- [20] H.-C. Zhou, J.R. Long, O.M. Yaghi, Introduction to Metal-Organic Frameworks, ACS Publications, 2012, pp. 673–674.
- [21] H. Poursadegh, M.S. Amini-Fazl, S. Javanbakht, F. Kazeminava, Magnetic nanocomposite through coating mannose-functionalized metal-organic framework with biopolymeric pectin hydrogel beads: a potential targeted anticancer oral delivery system, Int. J. Biol. Macromol. 254 (2024) 127702.
- [22] B.A. Lakshmi, S. Kim, Current and emerging applications of nanostructured metal-organic frameworks in cancer-targeted theranostics, Mater. Sci. Eng. C 105 (2019) 110091.
- [23] Z. Luo, S. Fan, C. Gu, W. Liu, J. Chen, B. Li, J. Liu, Metal-organic framework (MOF)-based nanomaterials for biomedical applications, Curr. Med. Chem. 26 (18) (2019) 3341–3369.
- [24] S.T. Meek, J.A. Greathouse, M.D. Allendorf, Metal-organic frameworks: a rapidly growing class of versatile nanoporous materials, Adv. Mater. 23 (2) (2011) 249–267
- [25] B. Yan, Lanthanide-functionalized metal-organic framework hybrid systems to create multiple luminescent centers for chemical sensing, Accounts Chem. Res. 50 (11) (2017) 2789–2798.
- [26] H.F. El Sharif, F. Giosia, S.M. Reddy, Investigation of polyacrylamide hydrogel-based molecularly imprinted polymers using protein gel electrophoresis, J. Mol. Recogn. 35 (1) (2022) e2942.
- [27] R.A. Almotiri, K.J. Ham, V.M. Vijayan, S.A. Catledge, Molecularly imprinted polyacrylamide with fluorescent nanodiamond for creatinine detection, Materials 12 (13) (2019) 2097.
- [28] M.A. Abd El-Aal, M.A. Al-Ghobashy, F.A.A. Fathalla, Y.S. El-Saharty, Preparation and characterization of pH-responsive polyacrylamide molecularly imprinted polymer: application to isolation of recombinant and wild type human serum albumin from biological sources, J. Chromatogr. B 1046 (2017) 34–47.
- [29] S. Han, Y. Song, S. Liu, L. Zhao, R. Sun, Dual responsive molecularly imprinted polymers based on UiO-66-DOX for selective targeting tumor cells and controlled drug release, Eur. Polym. J. 171 (2022) 111219.
- [30] S. Han, A. Yao, Y. Ding, Q. Leng, F. Teng, L. Zhao, R. Sun, H. Bu, A dual-template imprinted polymer based on amino-functionalized zirconium-based metal-organic

- framework for delivery of doxorubicin and phycocyanin with synergistic anticancer effect, Eur. Polym. J. 170 (2022) 111161.
- [31] S. Patra, N.N. Bala, G. Nandi, Synthesis, characterization and fabrication of sodium carboxymethyl-okra-gum-grafted-polymethacrylamide into sustained release tablet matrix, Int. J. Biol. Macromol. 164 (2020) 3885–3900.
- [32] M. Aydın, E.B. Aydın, M.K. Sezgintürk, A highly selective poly (thiophene)-graft-poly (methacrylamide) polymer modified ITO electrode for neuron specific enolase detection in human serum, Macromol. Biosci. 19 (8) (2019) 1900109.
- [33] E. Abdollahi, A. Khalafi-Nezhad, A. Mohammadi, M. Abdouss, M. Salami-Kalajahi, Synthesis of new molecularly imprinted polymer via reversible addition fragmentation transfer polymerization as a drug delivery system, Polymer 143 (2018) 245–257.
- [34] X. Fu, Q. Yang, Q. Zhou, Q. Lin, C. Wang, Template-monomer interaction in molecular imprinting: is the strongest the best? Open J. Org. Polym. Mater. 5 (2) (2015) 58.
- [35] S. Javanbakht, A. Saboury, A. Shaabani, R. Mohammadi, M. Ghorbani, Doxorubicin imprinted photoluminescent polymer as a pH-responsive nanocarrier, ACS Appl. Bio Mater. 3 (7) (2020) 4168–4178.
- [36] H. Hamedi, S. Javanbakht, R. Mohammadi, In-situ synthesis of copper-gallic acid metal-organic framework into the gentamicin-loaded chitosan hydrogel bead: a synergistic enhancement of antibacterial properties, J. Ind. Eng. Chem. 133 (2024) 454-463.
- [37] A. Saboury, R. Mohammadi, S. Javanbakht, M. Ghorbani, Doxorubicin imprinted magnetic polymethacrylamide as a pH-sensitive anticancer nanocarrier, J. Drug Deliv. Sci. Technol. 79 (2023) 103998.
- [38] N. Gowriboy, R. Kalaivizhi, N.J. Kaleekkal, M. Ganesh, K. Aswathy, Fabrication and characterization of polymer nanocomposites membrane (Cu-MOF@ CA/PES) for water treatment, J. Environ. Chem. Eng. 10 (6) (2022) 108668.
- [39] G. Zhan, L. Fan, F. Zhao, Z. Huang, B. Chen, X. Yang, S.f. Zhou, Fabrication of ultrathin 2D Cu-BDC nanosheets and the derived integrated MOF nanocomposites, Adv. Funct. Mater. 29 (9) (2019) 1806720.
- [40] B. Neises, W. Steglich, Simple method for the esterification of carboxylic acids, Angew Chem. Int. Ed. Engl. 17 (7) (1978) 522–524.
- [41] S. Javanbakht, A. Hemmati, H. Namazi, A. Heydari, Carboxymethylcellulose-coated 5-fluorouracil@ MOF-5 nano-hybrid as a bio-nanocomposite carrier for the anticancer oral delivery, Int. J. Biol. Macromol. 155 (2020) 876–882.
- [42] C. Luo, Q. Yang, X. Lin, C. Qi, G. Li, Preparation and drug release property of tanshinone IIA loaded chitosan-montmorillonite microspheres, Int. J. Biol. Macromol. 125 (2019) 721–729.
- [43] H. Yang, D.H. Bremner, L. Tao, H. Li, J. Hu, L. Zhu, Carboxymethyl chitosan-mediated synthesis of hyaluronic acid-targeted graphene oxide for cancer drug delivery, Carbohydr. Polym. 135 (2016) 72–78.
- [44] N.E. Tari, A. Tadjarodi, J. Tamnanloo, S. Fatemi, Synthesis and property modification of MCM-41 composited with Cu (BDC) MOF for improvement of CO2 adsorption Selectivity, J. CO2 Util. 14 (2016) 126–134.
- [45] S. Javanbakht, M. Pooresmaeil, H. Hashemi, H. Namazi, Carboxymethylcellulose capsulated Cu-based metal-organic framework-drug nanohybrid as a pH-sensitive nanocomposite for ibuprofen oral delivery, Int. J. Biol. Macromol. 119 (2018) 588-596.
- [46] C.G. Carson, K. Hardcastle, J. Schwartz, X. Liu, C. Hoffmann, R.A. Gerhardt, R. Tannenbaum, Synthesis and Structure Characterization of Copper Terephthalate Metal–Organic Frameworks, Wiley Online Library, 2009.
- [47] F. Parvinizadeh, A. Daneshfar, Fabrication of a magnetic metal-organic framework molecularly imprinted polymer for extraction of anti-malaria agent hydroxychloroquine, New J. Chem. 43 (22) (2019) 8508–8516.
- [48] F.B. Jahromi, A. Elhambakhsh, P. Keshavarz, F. Panahi, Insight into the application of amino acid-functionalized MIL-101 (Cr) micro fluids for high-efficiency CO2 absorption: effect of amine number and surface area, Fuel 334 (2023) 126603.
- [49] L. Li, L. Chen, H. Zhang, Y. Yang, X. Liu, Y. Chen, Temperature and magnetism biresponsive molecularly imprinted polymers: preparation, adsorption mechanism and properties as drug delivery system for sustained release of 5-fluorouracil, Mater. Sci. Eng. C 61 (2016) 158–168.
- [50] M. Cegłowski, J. Kurczewska, P. Ruszkowski, J. Liberska, G. Schroeder, The influence of cross-linking agent onto adsorption properties, release behavior and cytotoxicity of doxorubicin-imprinted microparticles, Colloids Surf. B Biointerfaces 182 (2019) 110379.
- [51] B.F. Shaw, H. Arthanari, M. Narovlyansky, A. Durazo, D.P. Frueh, M.P. Pollastri, A. Lee, B. Bilgicer, S.P. Gygi, G. Wagner, Neutralizing positive charges at the surface of a protein lowers its rate of amide hydrogen exchange without altering its structure or increasing its thermostability, J. Am. Chem. Soc. 132 (49) (2010) 17411–17425.
- [52] D. Shi, Cancer cell surface negative charges: a bio-physical manifestation of the Warburg effect, Nano Life 7 (03n04) (2017) 1771001.
- [53] B. Abdollahi, S. Farshnama, E.A. Asl, A. Najafidoust, M. Sarani, Cu (BDC) metal-organic framework (MOF)-based Ag2CrO4 heterostructure with enhanced solar-light degradation of organic dyes, Inorg. Chem. Commun. 138 (2022) 109236.
- [54] M. Celik, Preparation and characterization of starch-g-polymethacrylamide copolymers, J. Polym. Res. 13 (2006) 427–432.
- [55] D. Sinirlioglu, A. Aslan, A.E. Muftuoglu, A. Bozkurt, Synthesis and proton conductivity studies of methacrylate/methacrylamide-based azole functional novel polymer electrolytes, J. Appl. Polym. Sci. 131 (4) (2014).
- [56] S. Javanbakht, R. Mohammadian, H. Farhid, A. Shaabani, M.M. Amini, A green, reusable and remarkable catalyst for selective aerobic oxidation of alcohols: construction of Cu (BDC) on the surface of carboxymethyl cellulose fiber, Mater. Today Commun. 28 (2021) 102502.

- [57] S.A.S. Tabassi, S.V. Hashemi, S.A. Mohajeri, Dummy template molecularly imprinted polymer for omeprazole and the study of its drug binding and release properties, J. Appl. Polym. Sci. 130 (6) (2013) 4165–4170.
- [58] O.I. Parisi, C. Morelli, F. Puoci, C. Saturnino, A. Caruso, D. Sisci, G.E. Trombino, N. Picci, M.S. Sinicropi, Magnetic molecularly imprinted polymers (MMIPs) for carbazole derivative release in targeted cancer therapy, J. Mater. Chem. B 2 (38) (2014) 6619–6625.
- [59] F. Oroojalian, S. Karimzadeh, S. Javanbakht, M. Hejazi, B. Baradaran, T.J. Webster, A. Mokhtarzadeh, R.S. Varma, P. Kesharwani, A. Sahebkar, Current trends in stimuli-responsive nanotheranostics based on metal-organic frameworks for cancer therapy, Mater. Today 57 (2022) 192–224.
- [60] J.-E. Cun, X. Fan, Q. Pan, W. Gao, K. Luo, B. He, Y. Pu, Copper-based metal-organic frameworks for biomedical applications, Adv. Colloid Interface Sci. 305 (2022) 102686.
- [61] S. Dhanashree, M. Priyanka, K. Manisha, K. Vilasrao, Molecularly imprinted polymers: novel discovery for drug delivery, Curr. Drug Deliv. 13 (5) (2016) 632–645.
- [62] U. de Jesús Martín-Camacho, N. Rodríguez-Barajas, J.A. Sánchez-Burgos, A. Pérez-Larios, Weibull β value for the discernment of drug release mechanism of PLGA particles, Int. J. Pharm. 640 (2023) 123017.
- [63] A. Mohammadzadeh, S. Javanbakht, R. Mohammadi, F. Kazeminava, Ferrocenefunctionalized magnetic core-shell nanoparticles based on hydrosilylation reaction

- for pH-responsive doxorubic in delivery system, Colloids Surf. A Physicochem. Eng. Asp. $703\ (2024)\ 135201$.
- [64] A. Shaabani, R. Afshari, Synthesis of carboxamide-functionalized multiwall carbon nanotubes via Ugi multicomponent reaction: water-dispersible peptidomimetic nanohybrid as controlled drug delivery vehicle, ChemistrySelect 2 (18) (2017) 5218–5225.
- [65] Z. Chen, T. Shi, L. Zhang, P. Zhu, M. Deng, C. Huang, T. Hu, L. Jiang, J. Li, Mammalian drug efflux transporters of the ATP binding cassette (ABC) family in multidrug resistance: a review of the past decade, Cancer Lett. 370 (1) (2016) 153–164.
- [66] X. Pan, P. Li, L. Bai, J. Ma, S. Li, F. Zhang, S. Liu, Q. Wu, H. Shen, H. Liu, Biodegradable nanocomposite with dual cell-tissue penetration for deep tumor chemo-phototherapy, Small 16 (22) (2020) 2000809.
- [67] S. Darvishi, H. Hosseinzadeh, F. Kazeminava, A. Mahoutforoush, M. Tajik, M. Rasoulzadehzali, R. Mohammadi, S. Sadjadi, S. Javanbakht, Heparinfunctionalized Cu-based metal-organic framework: an efficient active and passive targeting nanocarrier for anticancer doxorubicin drug delivery, Int. J. Biol. Macromol. 282 (2024) 136648.
- [68] X. Zhang, S. Zhong, Y. Xu, D. Yu, T. Ma, L. Chen, Y. Zhao, X. Chen, S. Yang, Y. Wu, MicroRNA-3646 contributes to docetaxel resistance in human breast cancer cells by GSK-3β/β-catenin signaling pathway, PLoS One 11 (4) (2016) e0153194.